Nonlinear terahertz metamaterial perfect absorbers using GaAs [Invited]

Xiaoguang Zhao,[1,†] Jingdi Zhang,[2,†] Kebin Fan,[1] Guangwu Duan,[1] Grace D. Metcalfe,[3] Michael Wraback,[3] Xin Zhang,[1,*] and Richard D. Averitt[2,4]

[1]*Department of Mechanical Engineering, Boston University, 110 Cummington Mall, Boston, Massachusetts 02215, USA*
[2]*Department of Physics, University of California, San Diego, 9500 Gilman Dr., La Jolla, California 92093, USA*
[3]*Army Research Laboratory, 2800 Powder Mill Road, Adelphi, Maryland 20783, USA*
[4]*e-mail: raveritt@ucsd.edu*
**Corresponding author: xinz@bu.edu*

Received February 2, 2016; revised April 6, 2016; accepted April 25, 2016;
posted April 28, 2016 (Doc. ID 258715); published May 24, 2016

We investigate the nonlinear response of terahertz (THz) metamaterial perfect absorbers consisting of electric split ring resonators on GaAs integrated with a polyimide spacer and gold ground plane. These perfect absorbers on bulk semi-insulating GaAs are characterized using high-field THz time-domain spectroscopy. The resonance frequency redshifts 20 GHz and the absorbance is reduced by 30% as the incident peak field is increased from 30 to 300 kV/cm. The nonlinear response arises from THz field driven interband transitions and intervalley scattering in the GaAs. To eliminate the Fresnel losses from the GaAs substrate, we design and fabricate a flexible metamaterial saturable perfect absorber. The ability to create nonlinear absorbers enables appealing applications such as optical limiting and self-focusing.

OCIS codes: (040.2235) Far infrared or terahertz; (160.3918) Metamaterials; (160.4330) Nonlinear optical materials.
http://dx.doi.org/10.1364/PRJ.4.000A16

1. INTRODUCTION

The development of metamaterials provides a novel route to control light–matter interactions across the spectrum from microwave to visible frequencies [1]. Even though metamaterials have been primarily designed as linear response effective media, significant nonlinearities occur when appropriate materials are judiciously integrated into the active regions of split ring resonators [2]. Importantly, near-field enhancement within the unit cells can enhance the nonlinearity arising from the substrate material [3–5]. This has enabled applications such as second-harmonic generation [6,7] and self-reconfigurable chirality [8], among others [9].

There have been pioneering demonstrations of nonlinear metamaterials at microwave frequencies [3], extending to the IR [10]. With the rapid development of intense terahertz (THz) sources, nonlinear THz metamaterials have attracted great interest [11]. As with other spectral regions, THz metamaterials can confine the electric or magnetic field to subwavelength dimensions, yielding pronounced field enhancement [12,13]. This enables phenomena such as field-induced phase transitions [14], ultrafast field emission of electrons [15,16], electromigration [17], and electroluminescence [18]. Quite generally, nonlinear THz metamaterials can be realized by integrating subwavelength resonators with transition metal oxides [14], semiconductors [18–20], or any other nonlinear dielectric medium. GaAs, as a direct band semiconductor material, exhibits a significant nonlinear response due to field-induced carrier dynamics [21–23]. It has been used to demonstrate the nonlinear metamaterials, as described in Refs. [18,19].

In this paper, we present nonlinear metamaterial perfect absorbers (MPAs), which couple to both the electric and magnetic fields of the THz pulses. We investigate the nonlinear properties of a solid MPA on a bulk GaAs substrate and a flexible ultrathin MPA. For the solid MPA, the *LC* resonance frequency redshifts about 20 GHz and the peak absorption decreases from 100% to 70% as the incident THz peak electric field is increased from 30 to 300 kV/cm. For the flexible MPA, the absorption decreases with an increase in the peak field strength and exhibits a saturation behavior when the peak field exceeds 210 kV/cm. Based on numerical simulation of carrier dynamics, we conclude that the nonlinear response originates from the field-induced carrier generation and intervalley scattering (IVS) in the GaAs.

2. NONLINEAR THZ METAMATERIAL PERFECT ABSORBER ON SOLID SUBSTRATE

A. Design and Fabrication

The nonlinear THz MPA consists of an array of electric split ring resonators (ESRRs) on the semi-insulating GaAs (SI-GaAs) substrate, a polyimide (PI) spacer, and a gold ground plane (GND) [Fig. 1(a)]. The absorption (A) of the MPA can be calculated with the experimental transmission coefficient (t) and reflection coefficient (r) according to

$$A = 1 - |t|^2 - |r|^2. \quad (1)$$

The reflection from the MPA can be analyzed with interference theory [24–26]. When the THz pulse impinges on the metamaterial from the GaAs substrate, a fraction of

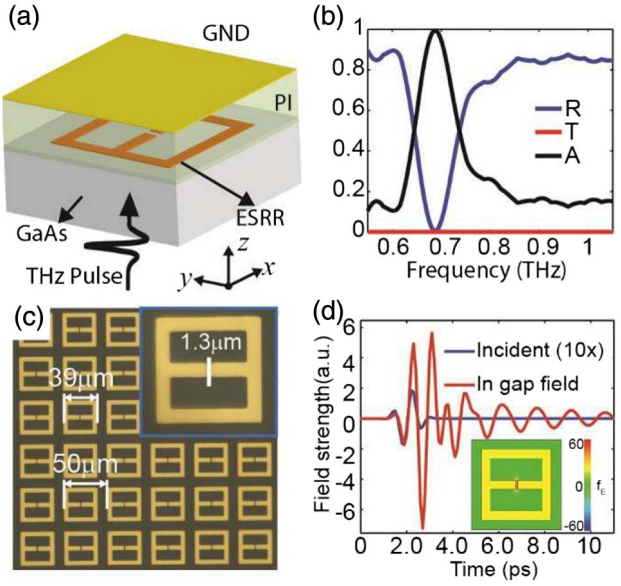

Fig. 1. (a) Schematic of the MPA on the GaAs substrate; (b) simulated transmission (T), reflection (R), and absorption (A) spectra; (c) microscope image of the ESRR array of the MPA (inset: close-up view of a unit cell); (d) simulated time domain field strength of the incident THz pulse (10×) and the electric field in the middle of the capacitive gap [inset: the 2D map of the electric field enhancement factor (f_E)].

the electromagnetic (EM) wave will be reflected due to the induced currents in the ESRR, which is accounted for by the complex reflection coefficient $\check{r}_{12}$. The remaining portion will be transmitted into the spacer layer with the complex transmission coefficient $\check{t}_{12}$. The transmitted light will be totally reflected by the GND after traveling in the PI spacer. Multiple reflections occur in the spacer, and the total reflection from the MPA can be expressed by [25]

$$r = \check{r}_{12} - \frac{\check{t}_{12}\check{t}_{21}e^{i2\beta}}{1 + \check{r}_{21}e^{i2\beta}}, \tag{2}$$

where β is the phase delay in the spacer and $\beta = nk_0d$, in which n is the refractive index of the spacer, k_0 is the free space wavenumber, and d is the spacer thickness. For each metamaterial structure, we can find an optimized spacer thickness to cancel out the reflection due to the destructive interference, i.e., $r = 0$ (at certain frequency bands). At the same time, the transmission is blocked by the ground plane ($t = 0$). As a result, the EM wave is absorbed by the MPA at these frequency bands. For instance, we can achieve near-perfect absorption at 0.7 THz [Fig. 1(b)] with the metamaterial structure shown in Fig. 1(c). In this design, the ESRR unit cells have a side width of 39 μm, capacitive gap of 1.3 μm, thickness of 150 nm, periodicity of 50 μm, and 5.5 μm thick PI spacer.

According to the simulation results shown in Fig. 1(d), the peak field in the 1.3 μm capacitive gap is enhanced by a factor of 30 in comparison to the incident field. The enhancement factor is larger than the metamaterials that only couple the incident electric field [18,19]—i.e., in comparison to ESRRs not configured into a perfect absorber geometry. In the MPA structure, multiple reflections of the THz pulse in the spacer layer induce surface currents in the ESRRs. On resonance these currents add constructively, resulting in a higher field enhancement in the capacitive gaps than for the case of single-layer ESRRs. The intense in-gap electric field can induce electron tunneling and/or impact ionization (IMI) in the semiconductor substrate, modifying the electronic properties of the substrate in the vicinity of the gap. This, in turn, changes the EM response of the MPA. Hence, a nonlinear perfect absorber for which the EM characteristics depend on the incident field strength is expected.

The MPA was fabricated using standard surface micromachining techniques [19]. The ESRRs were patterned on the SI-GaAs substrate with subsequent processes of photolithography, e-beam deposition of gold, and lift-off. Then, the PI spacer was spin coated and cured at 275°C in N_2 ambient, followed by GND deposition.

B. Results and Discussion

The MPA is characterized using high-field THz time-domain spectroscopy (TDS) in reflection [27]. Intense THz pulses with a maximum peak electric field of 300 kV/cm are generated using the tilted-pulse-front technique in $LiNbO_3$ [28]. A pair of wire grid polarizers are used to control the electric field strength (from 30 to 300 kV/cm) and polarization. Due to the existence of the GND, we have to probe the MPA from the back side of the GaAs substrate. As such, there is a front surface reflection from the GaAs in addition to multiple reflections (Fabry–Perot reflections) in the GaAs substrate, as depicted in Fig. 2(a). In the temporal response of the solid MPA sample, the first pulse corresponds to the reflection at the air/substrate interface. The pulse that interacts with the MPA is the second one in the time-domain data. Thus, in what follows for the bulk absorber, we measure the *internal absorption* and neglect the reflective losses of the bulk substrate [27,29,30]. For proper characterization, a piece of SI-GaAs coated with the PI spacer and GND is used as the reference [Fig. 2(b)]. We perform the Fourier transform on the second pulse in the reflection of the MPA sample (the pulse in the gray area in Fig. 2) to get the spectrum and normalize it to the spectrum of the second pulse of the reference.

The experimental reflection spectra of the MPA are shown in Fig. 3. The reflection (r) is measured at different incident

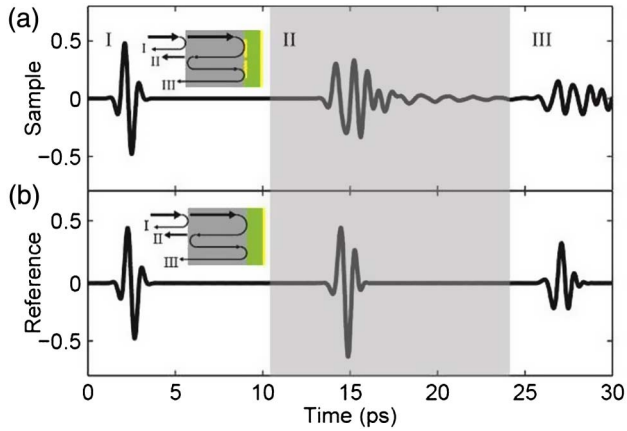

Fig. 2. Simulated time-domain response of (a) the MPA and (b) the reference demonstrates the multi-reflection effect of the GaAs substrate. The second pulse (gray shaded area) is the internal absorption response that is considered in our analysis.

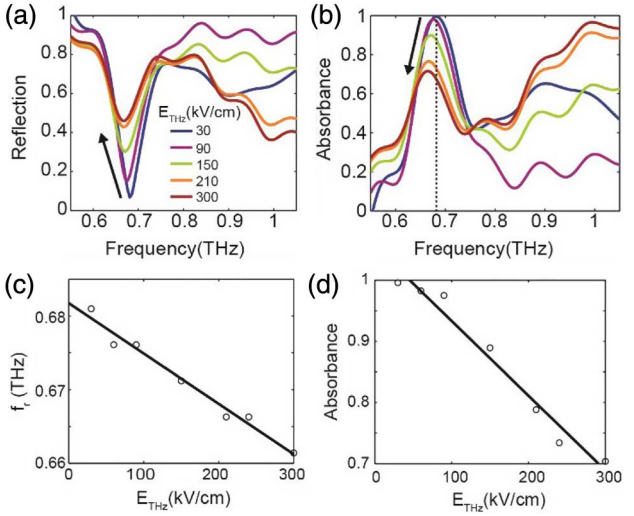

Fig. 3. (a) Measured reflection spectra of the nonlinear MPA under different THz field strengths, (b) calculated nonlinear absorbance spectra, (c) the resonance frequency versus the incident THz peak field, (d) the absorbance at 0.68 THz versus the incident THz peak field.

THz field strengths. The ground plane eliminates the transmission (t). The absorbance (A) is calculated according to Eq. (1). At low incident THz electric fields, the maximum absorption is achieved at 0.68 THz, corresponding to the LC resonance mode of the metamaterial. With an increasing electric field, the LC mode shifts to lower frequencies; at the same time, the peak absorption is suppressed, as is plotted in Figs. 3(c) and 3(d). Our device behaves like a saturable absorber. The nonlinear response of the MPA originates from the field-dependent carrier dynamics in the substrate as described below.

The substrate used in the MPA is SI-GaAs with low carrier density ($\sim 1\times 10^7$ cm^{-3}) [31]. Upon high field THz illumination, electrons are injected into the conduction band in the SI-GaAs substrate in the vicinity of each ESRR gap, causing a decrease in absorption. We can determine whether multiphoton absorption or tunneling ionization dominates the transition by using the Keldysh parameter [32] $\gamma_K = \omega_{\mathrm{THz}}\sqrt{2m^*E_g}/(eE_{n,\max})$, where ω_{THz} and $E_{n,\max}$ are, respectively, the frequency and peak field strength of the in-gap THz field; m^* and E_g are the effective electron mass and bandgap of GaAs, respectively; e is the electron charge. For instance, when the incident peak field is 90 kV/cm, $E_{n,\max}$ is ~2.7 MV/cm in the middle of the gap using the field enhancement determined from the simulation [Fig. 1(d)]. We use the resonance frequency (0.68 THz) to calculate of the Keldysh parameter, yielding $\gamma_K \approx 0.02 \ll 1$. This indicates a location deep in the tunneling ionization regime and that multiphoton absorption (not surprisingly) plays no role in carrier generation.

Nonetheless, there are two possible mechanisms for THz-induced carrier generation: IMI and Zener tunneling [18,23]. Efficient IMI occurs when the carrier kinetic energy exceeds the threshold energy $E_{\mathrm{th}} = E_g(2m^* + m_{hh})/m^* + m_{hh} =$ 1.6 eV where m^* and m_{hh} are, respectively, the effective masses of electrons and heavy holes [33]. In the absence of scattering, the process of the IMI can be modeled using $\hbar dk/dt = -eE_n(t)$, where k is the electron momentum and E_n is the enhanced in-gap THz electric field. When k reaches the threshold value $\pm 2.7\times 10^9$ m^{-1}, IMI is initiated and k goes to 0 based on the assumption that the electrons lose all of their kinetic energy after IMI [23]. N generations of IMI will lead to an increase in the electron density by a factor of 2^N. Based on our simulated in-gap electric field, the above equation yields an increase in the carrier density of $\sim 10^3$ during a half-cycle of the THz pulse for an incident field of $E_{\mathrm{THz}} = 30$ kV/cm. At higher incident fields (e.g., $E_{\mathrm{THz}} = 300$ kV/cm), the predicted carrier density increase is many orders of magnitude greater. However, the results clearly overestimate the final carrier density, since the velocity saturation due to collisions with defects, etc., is not included. Nonetheless, we cannot exclude the contribution of IMI to carrier generation.

For Zener tunneling, we can calculate the tunneling rate using

$$r_z = \frac{e^2E_n^2m_r^{1/2}}{18\pi\hbar^2E_g^{1/2}}\exp\left(\frac{-\pi m_r^{1/2}E_g^{3/2}}{2\hbar eE_n}\right), \tag{3}$$

where $m_r = 0.059m_0$ is the reduced mass accounting for the creation of electron heavy-hole pairs [18]. With an in-gap peak electric field of 9 MV/cm, r_z is on the order of 1×10^{18} (cm^3 fs)$^{-1}$. Considering the limited density of states in the conduction band ($\sim 4.7\times 10^{17}$ cm^{-3}), both IMI and Zener tunneling are great enough to substantially increase the conduction band population within a half-cycle of the driving field. As such, it is hard to conclude which mechanism is dominant. A complete understanding of the process of the carrier proliferation is beyond the scope of this work and requires more effort. For example, saturation due to Pauli exclusion needs to be considered. The electroluminescence spectrum [18] and temperature-dependent nonlinearities [20] may facilitate estimates of the ionization rate and aid in identifying the dominant carrier generation mechanism. However, the current analysis (and more importantly, experimental results) is sufficient to conclude that the carrier density of the in-gap GaAs increases significantly under high field THz excitation.

Besides the carrier density increase, IVS is induced by the enhanced THz electric field [19]. Electrons that are accelerated to an energy of ~1 eV can scatter from the Γ valley to the L valley [34]. The electrons in the Γ valley have a mobility of 4200 cm^{-2} • s^{-1} V^{-1}, while those in the L valley have a mobility of 400 cm^{-2} • s^{-1} V^{-1}. Thus, in-gap IVS will also affect the nonlinear response of the MPA. In short, IMI and Zener tunneling increase the carrier density, while IVS leads to a reduction in the carrier mobility.

To qualitatively understand the nonlinearity in the MPA, we use the finite-difference time-domain simulation with CST Microwave Studio to reproduce the experimental results. In the simulation, the conductivity of gold is 4.5×10^5 S/cm, and the PI is treated as a lossy dielectric material with a permittivity of 2.88 and loss tangent of 0.032. We model the GaAs with the Drude model with permittivity given by

$$\varepsilon_{\mathrm{GaAs}} = \varepsilon_\infty - \frac{\omega_p^2}{\omega(\omega + i\gamma)}, \tag{4}$$

where $\varepsilon_\infty = 12.97$ is the permittivity of GaAs at infinite frequency, $\omega_p = \sqrt{ne^2/(\varepsilon_0 m^*)}$ is the plasma frequency, $\gamma = e/(m^*\mu)$ is the collision frequency, and μ is the mobility of the electrons. The initial carrier concentration in GaAs is

$n = 1.0 \times 10^7$ cm^{-3}, and the mobility is $\mu = 4200$ cm$^{-2} \bullet$ s^{-1} V^{-1}.

To accurately model the effect of high field THz carrier generation on the MPA response, the in-gap GaAs is modeled with three regions, as shown in the inset of Fig. 4(a). This approach is taken because the in-gap field is inhomogeneous [see the lower portion of Fig. 4(a)], being highest at the gap edges. As can be seen, the field enhancement factor at the edge of the gap is nearly 2 times larger than that at the center of the gap, meaning that it might be inaccurate if we model the in-gap GaAs as a homogeneous nonlinear material. To capture this spatial dependence, we divide the in-gap GaAs into three regions. Additionally, the thickness of the GaAs with field-modified properties is taken to be 0.5 μm. The regions near the gap edges [red in Fig. 4(a)] are taken to have a field-dependent carrier density (n_1, from Zener tunneling and IMI) and mobility (μ_1, from IVS). In contrast, the central region in the gap [brown in Fig. 4(a)] is to have a constant carrier density (n_2) of 1×10^{16} cm^{-3} and constant mobility (4200 cm$^{-2} \bullet$ s^{-1} V^{-1}). The value of 1×10^{16} cm^{-3} used is higher than the intrinsic carrier density of GaAs, because even the lowest incident field strength used in the experiment (30 kV/cm) is sufficient to modify carrier density [18].

The simulated reflection spectra with different n_1 and μ_1 values are shown in Fig. 4(b). We increase the carrier density (n_1) and decrease the mobility (μ_1) to reproduce the measured reflection spectra of the MPA, as shown in Fig. 3(a). The good agreement between simulation and experimental results indicates that our analysis of the free carrier generation and IVS is qualitatively correct. In addition, the redshift is accurately captured by taking into account the spatial nonlinearity of the gap. This isn't the case when we model the gap as homogeneous. We note that our simulations are quasi-static with the properties of the in-gap GaAs invariant in time, reflecting the average effect of the carrier dynamics that modulate the MPA response. In reality, the in-gap carrier dynamics change during the transit of THz pulses. The time dependence of the carrier generation processes and resultant evolution of the density and mobility are required for more accurate modeling. Nonetheless, our simulations capture the coarse-grained effect of nonlinear carrier generation on the MPA response.

One major limitation of this device is that the bulk GaAs introduces multiple reflections in the time-domain response. We will discuss an improved MPA without multiple reflections in the next section.

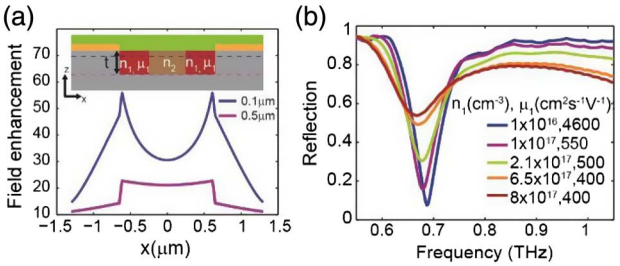

Fig. 4. (a) Simulated spatial distribution of the field enhancement across the gap at depths of 0.1 and 0.5 μm (inset: the cross section of the MPA), (b) simulated reflection spectra with different carrier densities and mobilities.

3. FLEXIBLE NONLINEAR THZ METAMATERIAL PERFECT ABSORBER

As shown in Fig. 5(a), we transfer the ESRRs with GaAs patches onto a flexible PI thin film using the semiconductor transfer technique described in [35]. The 200 nm AlGaAs and 400 nm SI-GaAs layers were subsequently epitaxially grown on the GaAs substrate. Square patches were etched out on the SI-GaAs layer, and the ESRRs were patterned on the patches. Then, the PI layer was spin coated and cured. Releasing holes were defined on the PI layer with photolithography and reactive ion etching. The SI-GaAs patches with ESRRs were transferred to the PI thin film by etching all of the AlGaAs sacrificial layer away using diluted HF solution. The last step was to coat the back side of the PI with a GND through e-beam evaporation. More details of the fabrication processes can be found in [35].

The fabricated MPA is as shown in Fig. 5(b). In each unit cell, the GaAs patch has a side width of 80 μm, on which there are two 44 μm by 12 μm release holes; the ESRR has a 68 μm side length, 2 μm capacitive gap, and 5 μm linewidth. The unit cells form an array with a periodicity of 100 μm. The metamaterial array and the ground plane are separated by a 16 μm thick PI spacer. The fabricated flexible MPA can eliminate the Fabry–Perot effect from the bulk GaAs substrate. In this case, the THz pulses directly impinge on the substrate-free MPA structure and the reflection (Fig. 2) at the air–GaAs substrate interface is eliminated. According to simulations [Fig. 5(c)], the field enhancement factor in the flexible MPA is ~1.6 times stronger than that of the MPA fabricated on the bulk GaAs substrate. This is because of reduced screening of the electric field in the absence of the GaAs substrate.

The flexible MPA was attached onto a bare silicon substrate and characterized using high-field THz-TDS, in which a gold coated silicon chip was used as the reference. The experimental response of the flexible MPA was characterized under different incident field strengths, as plotted in Fig. 5(d). Due to the great field enhancement, a significant carrier density is generated at the lowest incident field, i.e., 30 kV/cm, resulting in an absorbance lower than the designed value of 100%. With

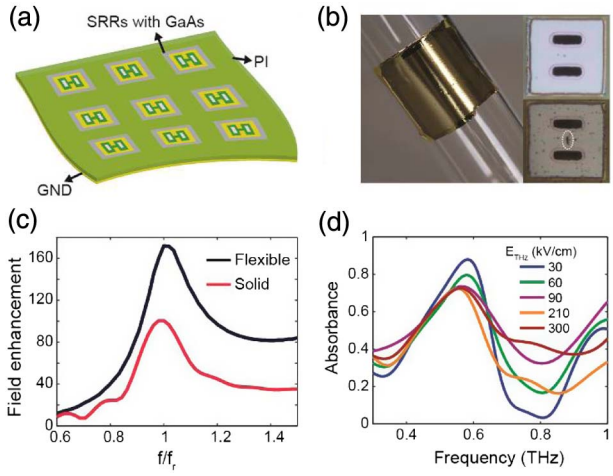

Fig. 5. (a) Illustration of the flexible MPA, (b) the fabricated MPA wrapped on a plastic vein [top inset: pristine unit cell; bottom inset: the unit cell damaged by the high field (the white circle highlights the damaged area)], (c) the field enhancement spectra of the flexible and solid MPAs, (d) measured absorbance at different field strengths.

the increase in the incident field, the absorbance at the resonance frequency is further suppressed due to the increasing carrier density. However, when the incident field exceeds 90 kV/cm, the change in resonance frequency and peak absorption slows down with the increase in the incident field strength. This suggests that the carrier density and mobility have saturated, preventing further changes in the response. It is different from the results of the aforementioned solid MPA, because the in-gap field is much larger in the flexible MPA. The in-gap GaAs is found to be damaged after the high-field THz exposure, as shown in the inset of Fig. 5(b), providing additional evidence of the stronger electric field. The breakdown of the semiconductor occurs due to a process similar to the avalanche breakdown of a reverse biased diode, where a large current driven by the electric field generates heat that damages the crystal structure permanently. At the same time, the lack of efficient thermal conduction in the flexible MPA may also contribute to the damage in the GaAs. After exposure to high-field THz pulses, the MPA does not return to a low-field response due to the permanent damage in GaAs. This permanent damage is absent in the solid MPA. This suggests that with additional design, it should be possible to create nonlinear flexible MPAs that operate at a significantly lower incident field.

4. CONCLUSION

We present the design, fabrication, and characterization of solid and flexible nonlinear MPAs based on the carrier dynamics in the GaAs. The metamaterials were designed to achieve near-unity absorption at a designated frequency and enhance the electric field, leading to carrier generation in the GaAs underneath the capacitive gaps of the ESRRs. In the solid MPA, a 20 GHz frequency shift and 30% absorbance reduction were measured when the incident field strength was increased from 30 to 300 kV/cm. In the flexible MPA, the Fabry–Perot effect from the GaAs substrate was eliminated and the saturated absorbance and GaAs damage were observed under a high-field condition due to the greater field enhancement. With careful structural design, the MPA can potentially realize a variety of functionalities, such as saturable absorption, optical limiting, and self-focusing.

ACKNOWLEDGMENT

This work was supported in part by the National Science Foundation under contract ECCS 1309835, and the DOE-Basic Energy Sciences under Grant No. DE-SC0012592. The authors would like to thank the Boston University Photonics Center for technical support.

†These authors contributed equally to this work.

REFERENCES

1. N. I. Zheludev and Y. S. Kivshar, "From metamaterials to metadevices," Nat. Mater. **11**, 917–924 (2012).
2. J. B. Pendry, A. J. Holden, D. Robbins, and W. Stewart, "Magnetism from conductors and enhanced nonlinear phenomena," IEEE Trans. Microwave Theory Tech. **47**, 2075–2084 (1999).
3. I. V. Shadrivov, A. B. Kozyrev, D. W. van der Weide, and Y. S. Kivshar, "Tunable transmission and harmonic generation in nonlinear metamaterials," Appl. Phys. Lett. **93**, 161903 (2008).
4. M. Lapine, I. V. Shadrivov, D. A. Powell, and Y. S. Kivshar, "Magnetoelastic metamaterials," Nat. Mater. **11**, 30-33 (2012).
5. A. P. Slobozhanyuk, M. Lapine, D. A. Powell, I. V. Shadrivov, Y. S. Kivshar, R. C. McPhedran, and P. A. Belov, "Flexible helices for nonlinear metamaterials," Adv. Mater. **25**, 3409–3412 (2013).
6. M. W. Klein, C. Enkrich, M. Wegener, and S. Linden, "Second-harmonic generation from magnetic metamaterials," Science **313**, 502–504 (2006).
7. K. O'Brien, H. Suchowski, J. Rho, A. Salandrino, B. Kante, X. Yin, and X. Zhang, "Predicting nonlinear properties of metamaterials from the linear response," Nat. Mater. **14**, 379–383 (2015).
8. J. Zhou, D. R. Chowdhury, R. Zhao, A. K. Azad, H.-T. Chen, C. M. Soukoulis, A. J. Taylor, and J. F. O'Hara, "Terahertz chiral metamaterials with giant and dynamically tunable optical activity," Phys. Rev. B **86**, 035448 (2012).
9. M. Lapine, I. V. Shadrivov, and Y. S. Kivshar, "Colloquium: nonlinear metamaterials," Rev. Mod. Phys. **86**, 1093–1123 (2014).
10. A. Minovich, J. Farnell, D. N. Neshev, I. McKerracher, F. Karouta, J. Tian, D. A. Powell, I. V. Shadrivov, H. H. Tan, and C. Jagadish, "Liquid crystal based nonlinear fishnet metamaterials," Appl. Phys. Lett. **100**, 121113 (2012).
11. G. Keiser, K. Fan, X. Zhang, and R. Averitt, "Towards dynamic, tunable, and nonlinear metamaterials via near field interactions: a review," J. Infrared Millim. Terahertz Waves **34**, 709–723 (2013).
12. M. Seo, H. Park, S. Koo, D. Park, J. Kang, O. Suwal, S. Choi, P. Planken, G. Park, and N. Park, "Terahertz field enhancement by a metallic nano slit operating beyond the skin-depth limit," Nat. Photonics **3**, 152–156 (2009).
13. C. A. Werley, K. Fan, A. C. Strikwerda, S. M. Teo, X. Zhang, R. D. Averitt, and K. A. Nelson, "Time-resolved imaging of near-fields in THz antennas and direct quantitative measurement of field enhancements," Opt. Express **20**, 8551–8567 (2012).
14. M. Liu, H. Y. Hwang, H. Tao, A. C. Strikwerda, K. Fan, G. R. Keiser, A. J. Sternbach, K. G. West, S. Kittiwatanakul, and J. Lu, "Terahertz-field-induced insulator-to-metal transition in vanadium dioxide metamaterial," Nature **487**, 345–348 (2012).
15. K. Iwaszczuk, M. Zalkovskij, A. C. Strikwerda, and P. U. Jepsen, "Nitrogen plasma formation through terahertz-induced ultrafast electron field emission," Optica **2**, 116–123 (2015).
16. J. Zhang, X. Zhao, K. Fan, X. Wang, G.-F. Zhang, K. Geng, X. Zhang, and R. D. Averitt, "Terahertz radiation-induced sub-cycle field electron emission across a split-gap dipole antenna," Appl. Phys. Lett. **107**, 231101 (2015).
17. A. C. Strikwerda, M. Zalkovskij, K. Iwaszczuk, D. L. Lorenzen, and P. U. Jepsen, "Permanently reconfigured metamaterials due to terahertz induced mass transfer of gold," Opt. Express **23**, 11586–11599 (2015).
18. C. Lange, T. Maag, M. Hohenleutner, S. Baierl, O. Schubert, E. Edwards, D. Bougeard, G. Woltersdorf, and R. Huber, "Extremely nonperturbative nonlinearities in GaAs driven by atomically strong terahertz fields in gold metamaterials," Phys. Rev. Lett. **113**, 227401 (2014).
19. K. Fan, H. Y. Hwang, M. Liu, A. C. Strikwerda, A. Sternbach, J. Zhang, X. Zhao, X. Zhang, K. A. Nelson, and R. D. Averitt, "Nonlinear terahertz metamaterials via field-enhanced carrier dynamics in GaAs," Phys. Rev. Lett. **110**, 217404 (2013).
20. A. T. Tarekegne, K. Iwaszczuk, M. Zalkovskij, A. C. Strikwerda, and P. U. Jepsen, "Impact ionization in high resistivity silicon induced by an intense terahertz field enhanced by an antenna array," New J. Phys. **17**, 043002 (2015).
21. W. Kuehn, P. Gaal, K. Reimann, M. Woerner, T. Elsaesser, and R. Hey, "Terahertz-induced interband tunneling of electrons in GaAs," Phys. Rev. B **82**, 075204 (2010).
22. F. Su, F. Blanchard, G. Sharma, L. Razzari, A. Ayesheshim, T. Cocker, L. Titova, T. Ozaki, J.-C. Kieffer, and R. Morandotti, "Terahertz pulse induced intervalley scattering in photoexcited GaAs," Opt. Express **17**, 9620–9629 (2009).
23. H. Hirori, K. Shinokita, M. Shirai, S. Tani, Y. Kadoya, and K. Tanaka, "Extraordinary carrier multiplication gated by a picosecond electric field pulse," Nat. Commun. **2**, 594 (2011).
24. H.-T. Chen, J. Zhou, J. F. O'Hara, F. Chen, A. K. Azad, and A. J. Taylor, "Antireflection coating using metamaterials and identification of its mechanism," Phys. Rev. Lett. **105**, 073901 (2010).
25. H.-T. Chen, "Interference theory of metamaterial perfect absorbers," Opt. Express **20**, 7165–7172 (2012).

26. L. Huang, D. R. Chowdhury, S. Ramani, M. T. Reiten, S.-N. Luo, A. K. Azad, A. J. Taylor, and H.-T. Chen, "Impact of resonator geometry and its coupling with ground plane on ultrathin metamaterial perfect absorbers," Appl. Phys. Lett. **101**, 101102 (2012).
27. H. R. Seren, J. Zhang, G. R. Keiser, S. J. Maddox, X. Zhao, K. Fan, S. R. Bank, X. Zhang, and R. D. Averitt, "Nonlinear terahertz devices utilizing semiconducting plasmonic metamaterials," arXiv: 1508.03183 (2015).
28. K.-H. Lin, C. A. Werley, and K. A. Nelson, "Nonlinear terahertz devices utilizing semiconducting plasmonic metamaterials," Appl. Phys. Lett. **95**, 103304 (2009).
29. H.-T. Chen, W. J. Padilla, J. M. O. Zide, A. C. Gossard, A. J. Taylor, and R. D. Averitt, "Active terahertz metamaterial devices," Nature **444**, 597–600 (2006).
30. H. R. Seren, G. R. Keiser, L. Cao, J. Zhang, A. C. Strikwerda, K. Fan, G. D. Metcalfe, M. Wraback, X. Zhang, and R. D. Averitt, "Optically modulated multiband terahertz perfect absorber," Adv. Opt. Mater. **2**, 1221–1226 (2014).
31. http://www.axt.com/site/index.php?q=node/38.
32. L. V. Keldysh, "Ionization in the field of a strong electromagnetic wave," Sov. Phys. JETP **20**, 1307–1314 (1965).
33. C. L. Anderson and C. R. Crowell, "Threshold energies for electron-hole pair production by impact ionization in semiconductors," Phys. Rev. B **5**, 2267–2272 (1972).
34. H. Bergner, V. Brückner, M. Lenzner, and R. Strobel, "Investigation of the field-dependent carrier mobility in GaAs by picosecond photoconductivity measurements," Phys. Stat. Sol. B **150**, 885–889 (1988).
35. X. Zhao, K. Fan, J. Zhang, H. R. Seren, G. D. Metcalfe, M. Wraback, R. D. Averitt, and X. Zhang, "Optically tunable metamaterial perfect absorber on highly flexible substrate," Sens. Actuators A **231**, 74–80 (2015).